

DOA ESTIMATION EXPLOITING INTERPOLATED MULTI-FREQUENCY SPARSE ARRAY

Shuimei Zhang*, Ammar Ahmed*, Yimin D. Zhang*, Shunqiao Sun†

* Department of Electrical and Computer Engineering, Temple University, Philadelphia, PA, USA

† Department of Electrical and Computer Engineering, The University of Alabama, Tuscaloosa, AL, USA

ABSTRACT

We consider gridless direction-of-arrival (DOA) estimation of much more targets than the number of physical sensors through the exploitation of multi-frequency sparse array design and processing which increase the degrees of freedom as more frequency components are used. A modified sensor interpolation technique is developed to accurately estimate the signal covariance matrix using very few snapshots, thereby eliminating the requirement of a large number of snapshots as in conventional different coarray-based DOA estimation. Simulation results demonstrate high-resolution gridless DOA estimation capability of more targets than the number of physical sensors.

Index Terms— Sparse array, multi-frequency sensing, array interpolation, direction-of-arrival estimation.

1. INTRODUCTION

Direction-of-arrival (DOA) estimation of targets is an important array signal processing area that finds broad applications in radar, sonar, wireless communications, navigation, radio astronomy, and seismology [1, 2]. Recently, there are significant renewed interests in underdetermined DOA estimation, i.e., determining the DOAs of more targets than the number of sensors. In particular, the recent development of systematic design of sparse arrays has generated a significant wave of interests in this area and resulted in new designs of sparse arrays and analyses of the achievable degrees of freedom (DOFs) and performance bounds (e.g., [3–15]). The essence behind these approaches is the utilization of the difference coarray concept, i.e., because DOA estimation deals with spatial power spectrum, we can utilize the autocorrelation function lags which have much more non-zero entries than the number of physical array sensors and thus can fill in missing positions in a sparse array. In general, sparse array design and processing may achieve $O(N^2)$ DOFs using only N sensors [16, 17]. A series of algorithms have been developed for effective DOA estimation using sparse arrays [18–23].

In [24], a novel concept of constructing a virtual coprime array using a single uniform linear array (ULA) through the exploitation of two frequencies with a coprime relationship was developed. This extends the coprime array concept into a joint spatio-spectral domain virtual array construction, thereby offering high flexibility in array design and achieving

much higher efficiency. The extension to more than two frequencies, high-order statistics, and the analysis of the achievable number of DOFs and DOA estimation performance are provided in [25–30].

Existing sparse array designs exploiting two or more frequencies suffer from two important issues: First, the formation of difference coarrays requires a high-accuracy covariance matrix estimate based on a large number of snapshots, which may not be applicable in many real-world applications (e.g., automotive radar [31]). Second, the use of ULA in coarray construction causes inherent lag redundancies, thereby reducing the achievable number of DOFs [12, 26].

In this paper, we develop a new multi-frequency sparse array framework to achieve high-resolution DOA estimation. First, the physical arrays are in general nonuniformly spaced to reduce lag redundancies. The processing scheme is based on modified array interpolation which, unlike difference coarray-based approaches that require a large number of snapshots, provides robust DOA estimation based on very few snapshots. The effectiveness of the proposed multi-frequency sparse array design and processing framework is illustrated using design examples and simulation results.

Notations: We use lower-case (upper-case) bold characters to describe vectors (matrices). In particular, I_L stands for the $L \times L$ identity matrix, and $(\cdot)^T$ and $(\cdot)^H$ respectively denote the transpose and conjugate transpose of a matrix or vector. $\|\cdot\|_*$ and $\|\cdot\|_F$ respectively represent the nuclear norm and Frobenius norm. Moreover, $|\cdot|$ denotes the cardinality of a set and \circ is the Hadamard product. In addition, $\mathcal{T}(\mathbf{x})$ denotes a Hermitian Toeplitz matrix with \mathbf{x} as its first column and $\text{Tr}(\cdot)$ represents the trace operator.

2. MULTI-FREQUENCY SPARSE ARRAY

2.1. Multi-Frequency Sparse Array Model

We consider a DOA estimation problem by simultaneously emitting I continuous wave signals with frequencies of $f_i, i = 1, 2, \dots, I$, from a single transmit antenna or a phased array. Extension to multiple transmitter cases is straightforward based on the multiple-input multiple-output (MIMO) radar concept [32]. Assume a virtual L_0 -sensor ULA with interelement spacing d . For the convenience of presentation and without loss of generality, the frequencies f_i are illustrated for the scenarios such that all M_i values are in-

tegers and satisfy $M_i \lambda_i / 2 = d$, where λ_i is the wavelength corresponding to f_i . Extension to multi-frequency sparse array designs involving fractional values will be reported separately.

The set \mathbb{S}_i containing the sensor positions for the i th frequency are expressed as:

$$\mathbb{S}_i = \{M_i l \bar{d} \mid l \in \mathbb{P}\}, \quad (1)$$

where $\mathbb{P} = \{0, 1, 2, \dots, L_0 - 1\}$ and \bar{d} denotes half-wavelength in a normalized frequency sense (i.e., no specific frequency is referred to).

For K far-field targets whose respective DOAs are $\theta_k, k = 1, 2, \dots, K$, the return signal vector associated with the i th frequency component is expressed as:

$$\tilde{\mathbf{x}}_{\mathbb{S}_i}(t) = e^{j2\pi f_i t} \sum_{k=1}^K \rho_k^i(t) \mathbf{a}_{\mathbb{S}_i}(\theta_k) + \tilde{\mathbf{n}}_{\mathbb{S}_i}(t), \quad (2)$$

where $\rho_k^i(t)$ is the reflection coefficient which is in general frequency-dependent because both phase delay and target reflectivity vary with frequency. In addition,

$$\mathbf{a}_{\mathbb{S}_i}(\theta_k) = \left[1, e^{-j \frac{2\pi d_1}{\lambda_i} \sin(\theta_k)}, \dots, e^{-j \frac{2\pi d_{L-1}}{\lambda_i} \sin(\theta_k)} \right]^T, \quad (3)$$

is the steering vector corresponding to θ_k , d_l is the physical location of the l th element with respect to the reference sensor, and L is the number of physical sensors. The sensor indexed by $l = 0$ is defined as the reference sensor, i.e., $d_0 = 0$. Furthermore, $\tilde{\mathbf{n}}_{\mathbb{S}_i}(t) \sim \mathcal{CN}(0, \sigma_n^i \mathbf{I}_L)$ denotes the additive white Gaussian noise.

After downconverting the received signal vector through separated low-pass filtering corresponding to each frequency component, we obtain the following baseband signal model:

$$\mathbf{x}_{\mathbb{S}_i}(t) = \sum_{k=1}^K \rho_k^i(t) \mathbf{a}_{\mathbb{S}_i}(\theta_k) + \mathbf{n}_{\mathbb{S}_i}(t) = \mathbf{A}_{\mathbb{S}_i} \boldsymbol{\rho}^i(t) + \mathbf{n}_{\mathbb{S}_i}(t), \quad (4)$$

where $\mathbf{A}_{\mathbb{S}_i} = [\mathbf{a}_{\mathbb{S}_i}(\theta_1), \dots, \mathbf{a}_{\mathbb{S}_i}(\theta_K)]$ and $\boldsymbol{\rho}^i(t) = [\rho_1^i(t), \dots, \rho_K^i(t)]^T$.

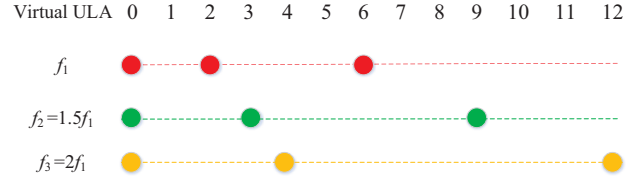
As we discussed earlier, difference coarray reconstruction based on a ULA inherently causes lag redundancies. Therefore, to achieve redundancy-free coarrays, we consider an L -sensor sparse array design by choosing l from $\mathbb{P}' \subset \mathbb{P}$ with cardinality $|\mathbb{P}'| = L < L_0$. In this case, the sensor locations for frequency f_i are given by:

$$\mathbb{S}_i = \{M_i l \bar{d} \mid l \in \mathbb{P}'\}. \quad (5)$$

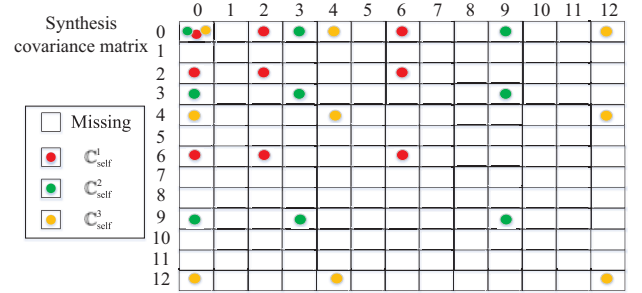
By incorporating the virtual sensors due to all I frequencies, we define the set \mathbb{S} of the combined sensor positions as:

$$\mathbb{S} = \bigcup_{i=1}^I \mathbb{S}_i = \bigcup_{i=1}^I \{M_i l \bar{d} \mid l \in \mathbb{P}'\}. \quad (6)$$

Note that the reference sensors of all I virtual arrays overlap at the zeroth position. Therefore, the number of unique virtual sensor positions is given by $|\mathbb{S}| \leq (L - 1)I + 1$, where the equality is achieved when all virtual sensors do not overlap except at the reference position.



(a) Configuration of multi-frequency sparse array



(b) Binary mask for covariance matrix interpolation

Fig. 1. Illustration of array configuration and binary mask for covariance matrix interpolation

2.2. Lag Analysis

Unlike coprime array interpolation discussed in [22, 23], the I virtual arrays in this paper share the same L sensors. On the other hand, the phase terms between $\mathbf{x}_{\mathbb{S}_i}(t)$ and $\mathbf{x}_{\mathbb{S}_j}(t)$, for $1 \leq i, j \leq I, i \neq j$, depend not only on the spatial angles of the impinging signals, but also on the unknown phase difference between the reflection coefficients $\rho_k^i(t)$ and $\rho_k^j(t)$ [24]. The existence of such unknown phase difference prohibits the direct utilization of the cross-lags obtained from the different frequency pairs, since $\rho_k^i(t)$ differs from $\rho_k^j(t)$ in general. Therefore, the array interpolation method developed in [22, 23] cannot be readily applied to the underlying DOA estimation problem.

Based on the fact that the self-lags corresponding to each single frequency component are not affected by the phase shift, we employ the self-lag set for the array interpolation purpose. The array interpolation is implemented by interpolating additional sensors into integer multiples of half-wavelength in the L_0 -element array. Note that the $|\mathbb{S}|$ unique virtual sensors resulting from I frequencies cannot be equivalently treated as $|\mathbb{S}|$ physical sensors due to the phase shift differences among different frequency pairs.

To have an intuitive understanding, we use a simple example of multi-frequency sparse array configuration with $I = 3$ frequencies as illustrated in Fig. 1(a). We set $f_2 = 1.5f_1$ and $f_3 = 2f_1$. The sensor positions for frequency f_1 is given as:

$$\mathbb{S}_1 = \{0, 2, 6\} \lambda_1 / 2, \quad (7)$$

i.e., $M_1 = 2$ and $\mathbb{P}' = \{0, 1, 3\}$. From the frequency ratios, we have $M_2 = f_2 M_1 / f_1 = 3$ and $M_3 = f_3 M_1 / f_1 = 4$. The

resulting virtual sensor positions corresponding to frequencies f_2 and f_3 are expressed as:

$$\mathbb{S}_2 = \{0, 3, 9\}\lambda_2/2, \quad \mathbb{S}_3 = \{0, 4, 12\}\lambda_3/2. \quad (8)$$

Collecting all virtual sensor positions and expressing them in terms of half-wavelength \bar{d} , regardless of the actual frequency, we obtain the collective sensor positions as:

$$\mathbb{S} = \mathbb{S}_1 \cup \mathbb{S}_2 \cup \mathbb{S}_3 = \{0, 2, 3, 4, 6, 9, 12\}\bar{d}. \quad (9)$$

The non-negative self-lag positions for the three frequency components are respectively expressed as $\mathbb{C}_{\text{self}}^1 = \{0, 2, 4, 6\}\bar{d}$, $\mathbb{C}_{\text{self}}^2 = \{0, 3, 6, 9\}\bar{d}$, and $\mathbb{C}_{\text{self}}^3 = \{0, 4, 8, 12\}\bar{d}$. The yielding non-negative self-lag positions are given as:

$$\mathbb{C}_{\text{self}}^+ = \{0, 2, 3, 4, 6, 8, 9, 12\}\bar{d}. \quad (10)$$

Note that this example involves redundant lags.

The received signals of the interpolated ULA can be initialized by augmenting $\mathbf{x}_{\mathbb{S}_i}(t)$ as

$$\langle \mathbf{y}_{\mathbb{U}}(t) \rangle_{\ell} = \begin{cases} \langle \mathbf{x}_{\mathbb{S}_i}(t) \rangle_{\ell}, & \ell \bar{d} \in \mathbb{S}_i, \\ 0, & \ell \bar{d} \in \mathbb{U} \setminus \mathbb{S}_i, \end{cases} \quad (11)$$

where $\mathbb{U} = \mathbb{P}\bar{d}$ and $\langle \cdot \rangle_{\ell}$ denotes the element corresponding to the sensor located at $\ell \bar{d}$ [7]. Accordingly, we define an L_0 -dimensional binary vector \mathbf{b}^i to describe the presence of virtual sensors indexed in the ULA \mathbb{U} . Elements of vector \mathbf{b}^i with value 1 imply the existence of virtual sensors with frequency f_i , whereas 0 stands for sensor positions to be interpolated, i.e.,

$$\langle \mathbf{b}^i \rangle_{\ell} = \begin{cases} 1, & \ell \bar{d} \in \mathbb{S}_i, \\ 0, & \ell \bar{d} \in \mathbb{U} \setminus \mathbb{S}_i. \end{cases} \quad (12)$$

We can initialize the received signals of the interpolated ULA $\mathbf{y}_{\mathbb{U}}(t)$ by

$$\mathbf{y}_{\mathbb{U}}^i(t) = \mathbf{x}_{\mathbb{U}}^i(t) \circ \mathbf{b}^i, \quad (13)$$

where $\mathbf{x}_{\mathbb{U}}^i(t)$ is the theoretical received signal for frequency f_i using the ULA and is modeled as follows:

$$\mathbf{x}_{\mathbb{U}}^i(t) = \sum_{k=1}^K \rho_k^i(t) \mathbf{a}_{\mathbb{U}}(\theta_k) + \mathbf{n}_{\mathbb{U}}^i(t) = \mathbf{a}_{\mathbb{U}} \boldsymbol{\rho}^i(t) + \mathbf{n}_{\mathbb{U}}^i(t). \quad (14)$$

Here, $\mathbf{a}_{\mathbb{U}}(\theta_k)$ is the array manifold vector of the interpolated ULA corresponding to the k th source and is expressed as:

$$\mathbf{a}_{\mathbb{U}}(\theta_k) = \left[1, e^{-j \frac{2\pi d_1}{\lambda_i} \sin(\theta_k)}, \dots, e^{-j \frac{2\pi d_{L_0-1}}{\lambda_i} \sin(\theta_k)} \right]^T. \quad (15)$$

In practice, the covariance matrix $\mathbf{R}_{\mathbf{y}_{\mathbb{U}}\mathbf{y}_{\mathbb{U}}}^i$ is unavailable and is approximated by its sample covariance matrix as:

$$\hat{\mathbf{R}}_{\mathbf{y}_{\mathbb{U}}\mathbf{y}_{\mathbb{U}}}^i = \frac{1}{T} \sum_{t=1}^T \mathbf{y}_{\mathbb{U}}^i(t) (\mathbf{y}_{\mathbb{U}}^i(t))^H, \quad (16)$$

where T is the number of snapshots. It is important to emphasize that the number of required snapshots can be very small for the proposed strategy (i.e., smaller than the number of sources or even a single snapshot can be utilized).

3. PROPOSED ARRAY INTERPOLATION AND DOA ESTIMATION

In this section, we propose a novel gridless DOA estimation algorithm based on multi-frequency sparse array interpolation. The concept of array interpolation is employed to generate the same aperture as the L_0 -sensor ULA. The unknown covariances are subsequently recovered via solving a convex optimization problem. The resulting covariance matrix enables to estimate more sources than the number of physical sensors, and the number of DOFs can be increased with more frequency components.

To enable effective information fusion of the covariance matrices associated with different frequencies, we define $\mathbf{B}^i = \mathbf{b}^i (\mathbf{b}^i)^T$ as the mask whose entries distinguish the known and unknown elements in $\hat{\mathbf{R}}_{\mathbf{y}_{\mathbb{U}}\mathbf{y}_{\mathbb{U}}}^i$. The synthesis covariance matrix exploiting the I frequencies is given by

$$\hat{\mathbf{R}}_{\mathbf{y}_{\mathbb{U}}\mathbf{y}_{\mathbb{U}}} = \left(\sum_{i=1}^I \hat{\mathbf{R}}_{\mathbf{x}_{\mathbb{U}}\mathbf{x}_{\mathbb{U}}}^i \circ \mathbf{B}^i \right) \circ \mathbf{D}, \quad (17)$$

where the (u, v) th element in \mathbf{D} for $(u, v) \in \{1, \dots, L_0\}^2$ denotes the inverse of the overlapping times, expressed as:

$$\mathbf{D}(u, v) = \frac{1}{\sum_{i=1}^I \mathbf{B}^i(u, v) + \epsilon}, \quad (18)$$

where ϵ is a small positive value in order to provide stability. Accordingly, the $L_0 \times L_0$ binary matrix \mathbf{B} distinguishing the known and unknown elements in $\hat{\mathbf{R}}_{\mathbf{y}_{\mathbb{U}}\mathbf{y}_{\mathbb{U}}}$ is

$$\mathbf{B} = \mathbf{D} \circ \sum_{i=1}^I \mathbf{B}^i. \quad (19)$$

For the design example illustrated in Fig. 1(a), the positions of the zero entries are represented by the empty boxes depicted in Fig. 1(b).

As indicated in [23], matrix completion fails to fill in the missing entries in $\hat{\mathbf{R}}_{\mathbf{y}_{\mathbb{U}}\mathbf{y}_{\mathbb{U}}}$ since several columns or rows are completely missing. Recall that the theoretical covariance matrix for a ULA has a Hermitian Toeplitz structure, and the number of targets is smaller than the number of sensors in the interpolated ULA, i.e., $K < L_0$. Therefore, we can reformulate the covariance matrix recovery problem as the following low-rank structured matrix completion problem:

$$\begin{aligned} \min_{\mathbf{w}} \quad & \text{rank}(\mathcal{T}(\mathbf{w})) \\ \text{s.t.} \quad & \left\| \mathcal{T}(\mathbf{w}) \circ \mathbf{B} - \hat{\mathbf{R}}_{\mathbf{y}_{\mathbb{U}}\mathbf{y}_{\mathbb{U}}} \right\|_F^2 \leq \delta, \\ & \mathcal{T}(\mathbf{w}) \succeq 0, \end{aligned} \quad (20)$$

where δ is the error tolerance. Note that the problem (20) is NP-hard. In the following, we relax the rank minimization objective by exploiting the nuclear norm minimization. As the nuclear norm of $\mathcal{T}(\mathbf{w})$ can be expressed as $\|\mathcal{T}(\mathbf{w})\|_* =$

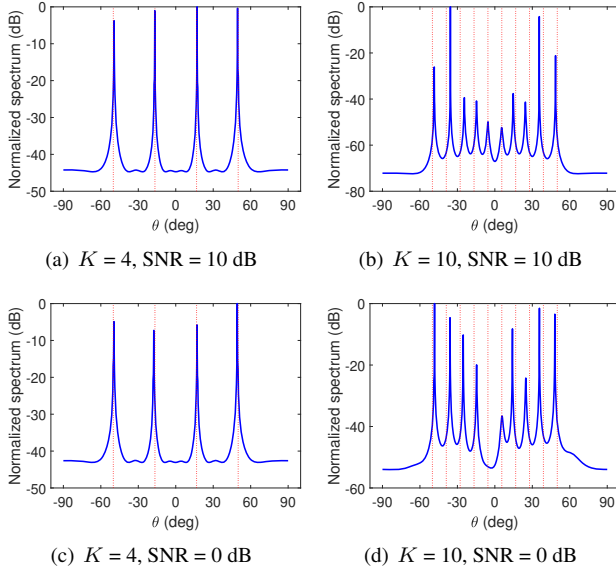


Fig. 2. DOA estimation results ($T = 9$).

$\text{Tr}(\sqrt{\mathcal{T}^H(\mathbf{w})\mathcal{T}(\mathbf{w})})$, we reformulate (20) as follows:

$$\begin{aligned} \min_{\mathbf{w}} \quad & \left\| \mathcal{T}(\mathbf{w}) \circ \mathbf{B} - \hat{\mathbf{R}}_{\mathbf{y}_U \mathbf{y}_U} \right\|_F^2 + \zeta \text{Tr} \left(\sqrt{\mathcal{T}^H(\mathbf{w})\mathcal{T}(\mathbf{w})} \right) \\ \text{s.t.} \quad & \mathcal{T}(\mathbf{w}) \succeq 0, \end{aligned} \quad (21)$$

where ζ is the regularization parameter. Note that the problem (21) is convex and can be solved using [33]. Subsequently, we exploit the MUSIC algorithm [34] to perform the DOA estimation, given its good trade-off between high resolution and computational simplicity. Other gridless DOA estimation methods, such as root-MUSIC and ESPRIT, can also be employed.

4. SIMULATION RESULTS

In this section, we present simulation results to demonstrate the DOA estimation performance of the proposed method for the design example described in Section 2.2. In this case, we have $|\mathcal{S}_i| = L = 3$ physical sensors. $|\mathcal{S}| = 7$ virtual sensors are obtained based on the use of $I = 3$ frequencies, and $|\mathcal{P}| = L_0 = 13$ sensors are rendered in the interpolated ULA. The regularization parameter ζ for covariance matrix recovery is set to 0.25.

K uncorrelated targets are assumed to be uniformly distributed in $[-50^\circ, 50^\circ]$. The noise power at the three frequencies are assumed to be the same, and the input SNR values for all sources are assumed to be identical. The phase difference between the received signal corresponding to different frequencies is independently and uniformly distributed in $[0, 2\pi]$. To verify the performance of the proposed method with few snapshots, only $T = 9$ data snapshots are used.

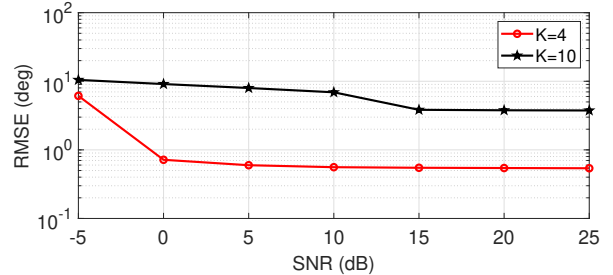


Fig. 3. RMSE versus SNR ($T = 9$).

Fig. 2 depicts the MUSIC pseudo-spectra. When the input SNR is 10 dB, as shown in Figs. 2(a) and 2(b), the proposed scheme successfully resolves both cases respectively with 4 and 10 targets, thus verifying the capability of the proposed method when the number of sources exceed the number of physical sensors and the number of snapshots. When SNR takes a lower value of 0 dB, the DOA estimation performance degrades. For the case of 4 targets, as shown in Fig. 2(c), the proposed algorithm remains effective to resolve all 4 targets. For the scenario with 10 targets, as shown in Fig. 2(d), most targets are still detected with one missing target.

We evaluate the performance of the proposed DOA estimation strategy in terms of root mean squared error (RMSE) for varying SNR. The RMSE is defined as follows:

$$\text{RMSE} = \sqrt{\frac{1}{NK} \sum_{n=1}^N \sum_{k=1}^K (\hat{\theta}_{k,n} - \theta_k)^2}, \quad (22)$$

where $\hat{\theta}_{k,n}$ denotes the estimate of the k th source θ_k in the n th Monte-Carlo trial. Fig. 3 shows the RMSE performance, obtained from 500 Monte-Carlo trials, with respect to the input SNR for both $K = 4$ and $K = 10$ cases. A lower RMSE value is obtained for the case with a smaller number of targets. We observe that the proposed algorithm has a floor at the high SNR region because of the small number of samples being used. For $K = 4$ and $K = 10$, the RMSE is respectively 0.5° and 3.5° at 20 dB input SNR with the use of 9 snapshots.

5. CONCLUSION

In this paper, we proposed a multi-frequency sparse array framework that can provide enhanced DOA estimation capability and resolve more targets than the number of physical sensors as well as the number of snapshots. The self-lags obtained at each frequency component are incorporated in a synthesis covariance matrix to achieve higher DOFs. A modified structured matrix completion scheme is developed to fill the missing entries in the resulting covariance matrix. Simulation results demonstrated that the proposed strategy provides promising performance for the DOA estimation especially for the case of less number of snapshots.

6. REFERENCES

- [1] H. L. Van Trees, *Detection, Estimation, and Modulation Theory, Part IV: Optimum Array Processing*. Wiley, 2002.
- [2] T. E. Tuncer and B. Friedlander (Eds.), *Classical and Modern Direction-of-Arrival Estimation*. Elsevier, 2009.
- [3] P. Pal and P. P. Vaidyanathan, "Nested arrays: A novel approach to array processing with enhanced degrees of freedom," *IEEE Trans. Signal Process.*, vol. 58, no. 8, pp. 4167–4181, Aug. 2010.
- [4] P. P. Vaidyanathan and P. Pal, "Sparse sensing with co-prime samplers and arrays," *IEEE Trans. Signal Process.*, vol. 59, no. 2, pp. 573–586, Feb. 2011.
- [5] P. Pal and P. P. Vaidyanathan, "Coprime sampling and the MUSIC algorithm," in *Proc. IEEE Digit. Signal Process. & Signal Process. Edu. Workshop*, Sedona, AZ, Jan. 2011, pp. 289–294.
- [6] S. Qin, Y. D. Zhang, and M. G. Amin, "Generalized coprime array configurations for direction-of-arrival estimation," *IEEE Trans. Signal Process.*, vol. 63, no. 6, pp. 1377–1390, March 2015.
- [7] C.-L. Liu and P. P. Vaidyanathan, "Cramér–Rao bounds for coprime and other sparse arrays, which find more sources than sensors," *Digital Signal Process.*, vol. 61, pp. 43–61, Feb. 2017.
- [8] A. Ahmed, Y. D. Zhang, and B. Himed, "Effective nested array design for fourth-order cumulant-based DOA estimation," in *Proc. IEEE Radar Conf.*, Seattle, WA, May 2017, pp. 998–1002.
- [9] W. Wang, S. Ren, and Z. Chen, "Unified coprime array with multi-period subarrays for direction-of-arrival estimation," *Digital Signal Process.*, vol. 74, pp. 30–42, March 2018.
- [10] C. Li, L. Gan, and C. Ling, "Coprime sensing via Chinese remaindering over quadratic fields — Part I: Array design," *IEEE Trans. Signal Process.*, vol. 67, no. 11, pp. 2898–2910, June 2019.
- [11] Z. Zheng, W.-Q. Wang, Y. Kong, and Y. D. Zhang, "MISC array: A new sparse array design achieving increased degrees of freedom and reduced mutual coupling effect," *IEEE Trans. Signal Process.*, vol. 67, no. 7, pp. 1728–1741, April 2019.
- [12] A. Ahmed, Y. D. Zhang, and J.-K. Zhang, "Coprime array design with minimum lag redundancy," in *Proc. IEEE ICASSP*, Brighton, U.K., May 2019, pp. 4125–4129.
- [13] Q. Shen, W. Liu, W. Cui, S. Wu, and P. Pal, "Simplified and enhanced multiple level nested arrays exploiting high-order difference co-Arrays," *IEEE Trans. Signal Process.*, vol. 67, no. 13, pp. 3502–3515, July 2019.
- [14] S. A. AlawshAli and H. Muqabel, "Achievable degree-of-freedom for three-level prime arrays," *Signal Process.*, vol. 171, no. 107523, pp. 1–8, June 2020.
- [15] S. Qin, Y. D. Zhang, and M. G. Amin, "Improved two-dimensional DOA estimation using parallel coprime arrays," *Signal Process.*, in press.
- [16] A. Moffet, "Minimum-redundancy linear arrays," *IEEE Trans. Antennas Propag.*, vol. 16, no. 2, pp. 172–175, March 1968.
- [17] R. T. Hoctor and S. A. Kassam, "The unifying role of the co-array in aperture synthesis for coherent and incoherent imaging," *Proc. IEEE*, vol. 78, no. 4, pp. 735–752, April 1990.
- [18] Y. D. Zhang, M. G. Amin, and B. Himed, "Sparsity-based DOA estimation using co-prime arrays," in *Proc. IEEE ICASSP*, Vancouver, Canada, May 2013, pp. 3967–3971.
- [19] Q. Shen, W. Liu, W. Cui, S. Wu, Y. D. Zhang, M. G. Amin, "Low-complexity direction-of-arrival estimation based on wideband co-prime arrays," *IEEE/ACM Trans. Audio, Speech Lang. Process.*, vol. 23, no. 9, pp. 1445–1456, Sept. 2015.
- [20] S. Qin, Y. D. Zhang, and M. G. Amin, "DOA estimation of mixed coherent and uncorrelated targets exploiting coprime MIMO radar," *Digital Signal Process.*, vol. 61, pp. 26–34, Feb. 2017.
- [21] C. Zhou, Y. Gu, Y. D. Zhang, Z. Shi, T. Jin, and X. Wu, "Compressive sensing based coprime array direction-of-arrival estimation," *IET Commun.*, vol. 11, no. 11, pp. 1719–1724, Aug. 2017.
- [22] C. Zhou, Y. Gu, X. Fan, Z. Shi, G. Mao, and Y. D. Zhang, "Direction-of-arrival estimation for coprime array via virtual array interpolation," *IEEE Trans. Signal Process.*, vol. 66, no. 22, pp. 5956–5971, Nov. 2018.
- [23] C. Zhou, Y. Gu, Z. Shi, and Y. D. Zhang, "Off-grid direction-of-arrival estimation using coprime array interpolation," *IEEE Signal Process. Lett.*, vol. 25, no. 11, pp. 1710–1714, Nov. 2018.
- [24] Y. D. Zhang, M. G. Amin, F. Ahmad, and B. Himed, "DOA estimation using a sparse uniform linear array with two CW signals of co-prime frequencies," in *Proc. IEEE Int. Workshop CAMSAP*, Saint Martin, Dec. 2013, pp. 404–407.
- [25] S. Qin, Y. D. Zhang, and M. G. Amin, "DOA estimation exploiting coprime frequencies," in *Proc. SPIE*, vol. 9103, no. 91030E, Baltimore, MD, May 2014.
- [26] S. Qin, Y. D. Zhang, M. G. Amin, and B. Himed, "DOA estimation exploiting a uniform linear array with multiple coprime frequencies," *Signal Process.*, vol. 130, pp. 37–46, Jan. 2017.
- [27] A. Ahmed, Y. D. Zhang, and B. Himed, "Cumulant-based direction-of-arrival estimation using multiple co-prime frequencies," in *Proc. Asilomar Conf. Signals, Syst., Comput.*, Pacific Grove, CA, Oct. 2017, pp. 1188–1192.
- [28] A. Liu, X. Zhang, Q. Yang, and W. Deng, "Fast DOA estimation algorithms for sparse uniform linear array with multiple integer frequencies," *IEEE Access*, vol. 6, pp. 29952–29965, May 2018.
- [29] M. Guo, Y. D. Zhang, and T. Chen, "Performance analysis for uniform linear arrays exploiting two coprime frequencies," *IEEE Signal Process. Lett.*, vol. 25, no. 6, pp. 838–842, June 2018.
- [30] M. Guo, Y. D. Zhang, and T. Chen, "Compressive measurements exploiting coprime frequencies for direction finding," in *Proc. IEEE Sensor Array and Multichannel Signal Process. Workshop*, Sheffield, U.K., July 2018, pp. 26–30.
- [31] S. Sun, A. P. Petropulu and H. V. Poor, "MIMO radar for ADAS and autonomous driving: Advantages and challenges," *IEEE Signal Process. Mag.*, in press.
- [32] J. Li and P. Stoica, *MIMO Radar Signal Processing*. Wiley, 2008.
- [33] M. Grant, S. Boyd, and Y. Ye, "CVX: MATLAB software for disciplined convex programming," 2009. Available: <http://www.stanford.edu/~boyd/cvx>.
- [34] R. O. Schmidt, "Multiple emitter location and signal parameter estimation," *IEEE Trans. Antennas Propag.*, vol. 34, no. 3, pp. 276–280, Mar. 1986.